

## Continuous discharge monitoring of the Mirim-São Gonçalo system by the index velocity rating curve method

George Marino Soares Gonçalves <sup>a</sup>, Guilherme Kruger Bartels <sup>b</sup>, Luciana Shigihara Lima <sup>c</sup>,  
Lukas dos Santos Boeira <sup>d</sup> and Gilberto Loguercio Collares <sup>e</sup>, \*

<sup>a</sup> Universidade Federal de Pelotas, Pelotas, Brazil

<sup>b</sup> UFRGS: Universidade Federal do Rio Grande do Sul, Pelotas, Brazil

<sup>c</sup> INPE: Instituto Nacional de Pesquisas Espaciais, São José Dos Campos, Brazil

<sup>d</sup> UFPEL: Universidade Federal de Pelotas, Pelotas, Brazil

<sup>e</sup> Engenharia Hídrica/Centro de Desenvolvimento Tecnológico, Universidade Federal de Pelotas, Gomes Carneiro, 01, Pelotas, Rio Grande do Sul 96010-610, Pelotas, Brazil

\*Corresponding author. E-mail: gilbertocollares@gmail.com

 GMSG, 0000-0003-2307-1875; GKB, 0000-0002-5060-9610; LSL, 0000-0001-7988-0853; LdS, 0000-0002-6139-5750; GLC, 0000-0003-4910-5420

### ABSTRACT

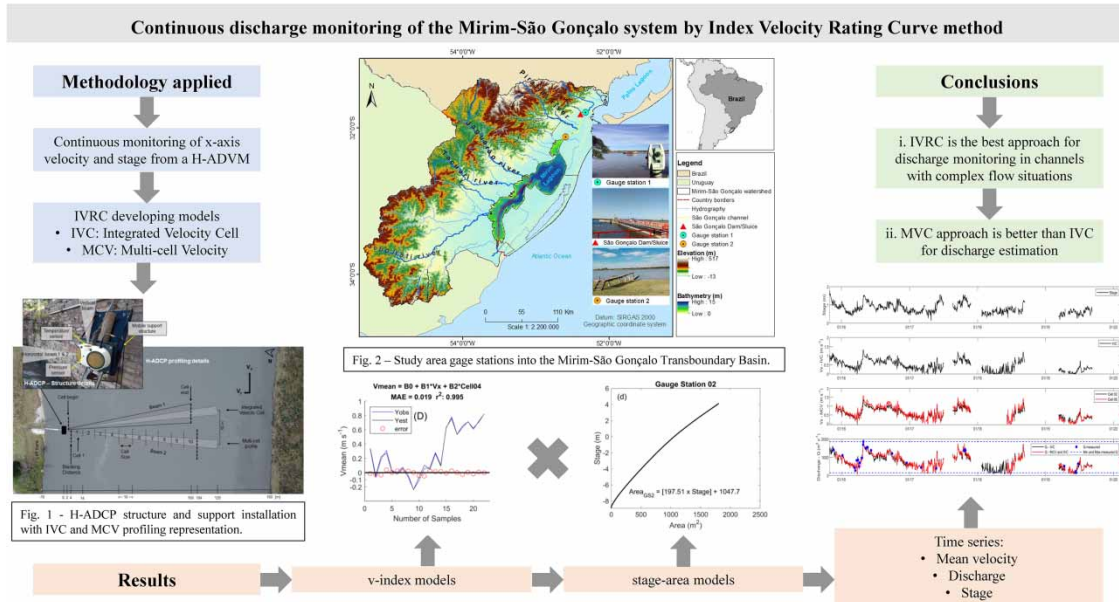
The São Gonçalo Channel, located in the south of Brazil, is responsible for connecting the Mirim Lagoon to the Patos Lagoon, constituting the largest coastal lagoon system in Latin America. The assessment of its hydraulic variables is necessary given the importance of this channel for the region. Thus, this study aimed to evaluate the performance of the index velocity rating curve (IVRC) method, from velocity measurements provided by horizontal static-type acoustic Doppler profilers (H-ADCPs). For the two sections analyzed in this study (GS1 and GS2), IVRC models were developed considering the integrated velocity cell (IVC) method; the multi-cell velocity (MCV) method; the joint use of IVC and MCV; and a stage-mean velocity rating curve. The results point to an  $r^2$  of 0.986 (IVC), 0.998 (IVC + MCV), 0.534 (stage-mean velocity) at GS1, and  $r^2$  of 0.986 (IVC), 0.995 (IVC + MCV), and 0.815 (stage-mean velocity) at GS2. In both GS1 and GS2, results showed significant gains – for different flow conditions – on continuous estimations of flow velocities and discharges when considering the MCV + IVC method. The IVRC model that presented the best fit allowed the development of a time-series of discharges in the studied sites with high reliability.

**Key words:** acoustic profiler, bi-directional flows, hydrodynamic, index velocity rating curve

### HIGHLIGHTS

- Assessment of the IVRC approaches on discharge estimations in a bi-directional natural channel.
- Increment of reliability while moving from an SQRC on discharge estimations to an IVRC approach.
- The possibility of registering complex flow situations from an *in situ* horizontal static-type ADPC.

## GRAPHICAL ABSTRACT



## NOTATIONS

SQRC	stage-discharge rating curve
IVRC	index velocity rating curve
ADCPs	acoustic Doppler current profilers
H-ADCP	horizontal acoustic Doppler current profiler
SGC	São Gonçalo Channel
GS1	gauge station 1
GS2	gauge station 2
IVC	integrated velocity cell
MCV	multi-cell velocity
D-ADCP	dynamic acoustic Doppler current profiler
MAE	mean absolute error
$V_{\text{D-ADCP}}$	cross-section water velocity from the D-ADCP
$V_{\text{mean}}$	cross-section water velocity from the IVRC model
$V_{\text{INDEX}}$	$x$ -axis index velocity

## INTRODUCTION

Covering approximately 13% of the world's coastal zones, coastal lagoons are characterized by a shallow water body, generally oriented parallel to the coast and separated from the ocean by a land barrier often affected by natural and anthropogenic aspects (Kjerfve 1994). The hydrodynamics in coastal lagoons is complex (Fiandrino *et al.* 2017), influenced by different forcings such as winds, tides, precipitation, and river discharge. Understanding the physical, chemical, geological, and ecological dynamics of these environments is an important task for the better adoption of coastal management strategies and planning in coastal lagoon areas (Kjerfve 1994).

The Patos-Mirim lagoon system is the largest coastal lagoon system in South America, having a 500 km long coastline (Oliveira *et al.* 2019). This system is considered complex due to the strong influence of wind action on the water level dynamics (Costi *et al.* 2018; Oliveira *et al.* 2019) causing multidirectional and stationary flow, as backwater effects. The north-east wind pushes the water into the southern portion of the Mirim Lagoon and disturbs the patterns of seasonal variability, resulting in water level oscillations (Costi *et al.* 2018), while the southerly winds push the water toward the north, raising the water level in that direction (Munar *et al.* 2018). When this region is under southwest wind influences, the Mirim Lagoon

flows toward the Patos Lagoon through the São Gonçalo Channel (SGC). Under the northeast wind influence, the SGC mouth's water level rises (Oliveira *et al.* 2019), causing inversive discharges.

All these reported dynamics directly influence the quality and availability of water, as well as the pollutants' residence time and navigability conditions in the Patos-Mirim lagoon system (Costi *et al.* 2018). Therefore, the continuous monitoring of water levels and flow discharges on this environment is relevant from both a social and economic perspective, as well as for the understanding of the hydrodynamic patterns of such a complex system. Among the used methods for continuous monitoring of the flows and consequent discharge estimations, the stage–discharge rating curve (SQRC) is the most common and traditional approach (Muste & Hoitink 2017; Cheng *et al.* 2019), and it is performed through a graphical and hydraulic analysis (WMO 1980; Dias *et al.* 2019). However, SQRCs are influenced by a minimum number of observations, and the stage–discharge relationship may vary over time, or even become impossible to determine especially in cases of backwater and inversive flow occurrence (Le Coz *et al.* 2008). Furthermore, in the SQRC approach, there is no distinction between the different hydrograph phases (rising and falling), since under unstable flow conditions, the hysteresis effects may occur between these two (stage and discharge) variables that are used to construct this relationship (Muste *et al.* 2020). In order to overcome the limitations imposed by the SQRC, the index velocity rating curve (IVRC) method relates the velocity at a specific point, the cross-section's mean velocity and wetted area to the stage, where the discharge value is the result from multiplying these relations (Chen *et al.* 2012). Thus, in complex flow situations, such as unstable and non-uniform flows, it is expected that the addition of permanent indexed velocity measurements will improve discharge estimates, due to the inclusion of flow dynamics information (Cheng *et al.* 2019).

While guidelines for developing SQRC are well known and extensively documented (e.g., WMO 1980; Rantz 1982a), the application of the IVRC has gained greater attention in recent decades, especially with the joint use of acoustic Doppler current profilers (ADCPs) (Levesque & Oberg 2012; Farahmand & Hamilton 2016). Continuous flow velocity measurements became possible since the implementation of horizontal acoustic Doppler current profilers (H-ADCPs), in a riverbank fixed position (Vougioukas *et al.* 2011). The H-ADCPs monitor the horizontal velocity profile in uniformly discrete intervals (cells) along the  $x$ -axis of the main beam (Vougioukas *et al.* 2011), at a specific flow depth (Kästner *et al.* 2018). Thus, the IVRC approach requires two models to estimate the discharge, one is the *stage–area* and the other is the *index velocity–mean velocity*. One of the main challenges in IVRC modeling is the model exploration and analysis in order to find the optimal regression model predictor(s) and model type (Farahmand & Hamilton 2016).

In recent years, many studies have been carried out in the Patos-Mirim lagoon system aiming to analyze, among other aspects, its environment hydrodynamics (Costi *et al.* 2018; Munar *et al.* 2018; Oliveira *et al.* 2019; Possa *et al.* 2022), the Mirim Lagoon residence time (Silva *et al.* 2019), spatial and seasonal water surface temperature variations (Munar *et al.* 2019), and the Mirim Lagoon bed sediment composition (Vieira *et al.* 2020). All these mentioned studies had used punctual *in situ* observed data (water velocity, current direction, discharge, stage) from the main Patos-Mirim lagoon system tributaries and the SGC, and also daily water level time-series from this region in their simulations and analyses. These studies evidence the lack of continuous monitoring programs involving equipment deployments and accurate techniques. Thus, continuous, accurate, and robust information regarding flow velocities, water discharges, and water level variation on a semi-daily scale are timely over this region.

Moreover, given the importance of this environment, both in terms of social and economic development, there is still no research investigating the best approach for IVRC use at the Patos-Mirim lagoon system and the SGC, despite the great potential of this territory, which covers an international transboundary basin shared between Brazil and Uruguay. Hence, this study assessed the performance of the IVRC method from applying velocity measurements provided by H-ADCPs, as a promising approach for continuous monitoring of flow velocities and discharges in a natural channel with typical complex flow characteristics. By analyzing discharge measurements under different flow conditions in two gauge stations along the SGC, on which H-ADCPs continuously monitor both gauges, we intend to answer the following questions:

- Is the rating curve traditional approach suitable for representing these flow conditions?
- Which IVRC development methods are most promising for representing the mean flow velocity at both gauge stations?

## MATERIALS AND METHODS

### Characterization of the study area

The Patos-Mirim lagoon system is in the extreme south of Brazil and east of Uruguay, encompassing the Patos and Mirim lagoons (Figure 1). These two lagoons have a total area of 13,749 km<sup>2</sup> (Vieira *et al.* 2020) where the Patos Lagoon comprises 10,000 km<sup>2</sup> (Munar *et al.* 2019) and Mirim Lagoon 3,749 km<sup>2</sup> (Toldo 1994; Friedrichf *et al.* 2006) and their only connection is made by the SGC. The SGC is a 76.6-km long natural channel with a mean depth of 6 m, maximum depth of 15 m, mean width of 250 m and a flood plain area that extends beyond the channel banks varying in range especially in the right banks (Figure 2), being the SGC responsible for draining the entire runoff from Mirim toward Patos. A dam and a navigation sluice were built in 1977 at the SGC to contain the backwater from Patos toward Mirim, thus avoiding saltwater intrusion in the southern portion of SGC and northern Mirim Lagoon. The mentioned dam operates opening/closing of 18 vertical moving gates, and its close/open periods depend primarily on the water levels and wind directions in this region. It guarantees freshwater for all the different uses in the southern portion of the watershed.

The Mirim-São Gonçalo Transboundary Basin (Figure 1) has an area of 62,250 km<sup>2</sup>, of which 29,250 km<sup>2</sup> is attached to the Brazilian territory, including 21 municipalities and an estimated population of 770,308 inhabitants, where 88.8% of the population lives in the urban area and 11.2% in the country area (SEMA 2021). In the Uruguayan side, the basin has an area of 33,000 km<sup>2</sup>, with a population of 154,699 which corresponds to 5% of the total population of the country, 92% living in urban areas and 8% in country areas (MVOTMA 2017). The main tributaries in the Brazilian territory are the Pelotas stream, the rivers Piratini and Jaguarão, and the SGC (Figure 1). On the Uruguayan side, the main rivers are Cebollati, Tacuari, Sarandi, and San Miguel. The climate of the Mirim-São Gonçalo basin region is characterized as humid subtropical (Cfa in the Köppen

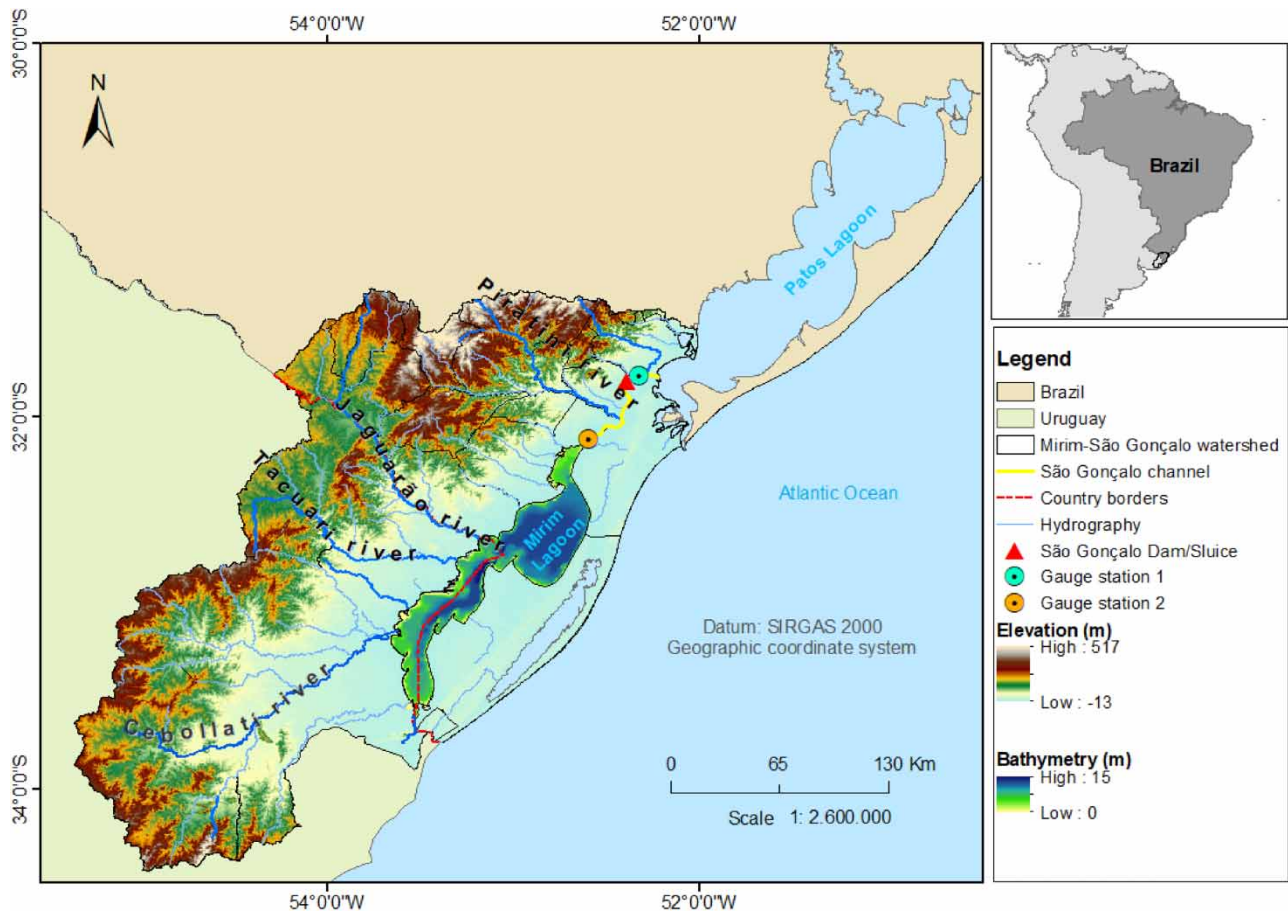


**Figure 1** | The Mirim-São Gonçalo transboundary basin location and its main tributaries, studied cross-sections, and the Patos-Mirim lagoon system.

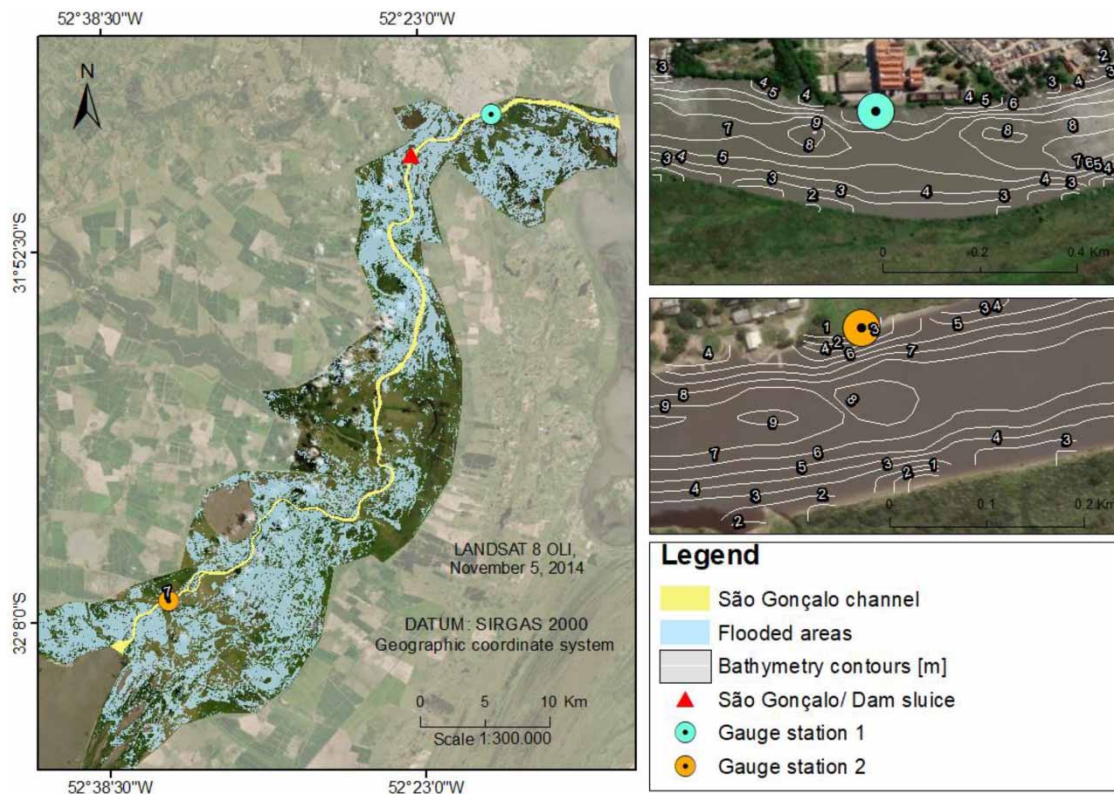


**Figure 2** | Flooded areas on a wet period in the São Gonçalo Channel, and locations of GS1, GS2, and São Gonçalo Dam/sluiice. The white lines represent the bathymetry contours in meters next to GS1/GS2 areas.

classification), with hot summers and well-distributed rainfall throughout the year (Peel *et al.* 2007). The annual precipitation in this region is  $1,400 \pm 296$  mm, the annual reference evapotranspiration is  $1,080 \pm 36$  mm, and the annual mean temperature is  $18.5 \pm 0.5$  °C (1971–2020).

The efforts to carry out the surveys were focused on two cross-sections (also called gauge stations) located at the two extremes of the SGC, 60 km apart from each other (Figure 2). The gauge station 1 (GS1) is in the Federal University of Pelotas, and it is about 10 km far from the SGC mouth, and this gauge has a mean width of 230 m and a mean depth of 6.1 m. The gauge station 2 (GS2) is in the Santa Isabel do Sul District, and it is about 4 km far from the Mirim Lagoon mouth, and this gauge has a mean width of 170 m and a mean depth of 7.6 m (an overview of GS1, São Gonçalo Dam/Sluice and GS2 are shown in Figure 3). In both monitored stations, a channel bed bathymetric survey was conducted applying a single-beam echo sounder model SDE-28S designed by SOUTH™/South Co., which has 200 kHz of frequency, and for the bank areas, a total station was applied, thus constituting the cross-sections of topobathymetry. The locations for the gauge's installations were chosen due to the accessibility and possibility of representing the SGC in its totality, as well for the equipment safety and the best hydraulic conditions as pointed out by Benson & Dalrymple (1967), Levesque & Oberg (2012) and Rantz (1982a). Flow velocity measurements were not carried in floodplains, due to the low flow depth and the presence of massive vegetation in flooded areas. These areas were not considered in the estimates of the cross-sections' wetted areas.

### Description of study site and ADCP installation

Water level and velocity were monitored on both gauge stations with H-ADCPs designed by SonTek™/YSI, model Argonaut Side-Looker (SL) of 500 kHz. The gauge stations were commissioned in October 2015 at GS1 and March 2018 at GS2. The H-ADCPs have two transducers and are mounted at one of the channel banks, aiming 'side-looking' toward the channel, providing a velocity measurement with an accuracy of  $0.005 \text{ m s}^{-1}$ . The horizontal beam width is  $1.4^\circ$  and its maximum profile long range is 120 m. The H-ADCPs comprise a built-in temperature sensor, a vertical beam, and a pressure sensor also used to monitor the water level. The equipment is direct current-powered through a solar panel and battery (~20 m of cable between

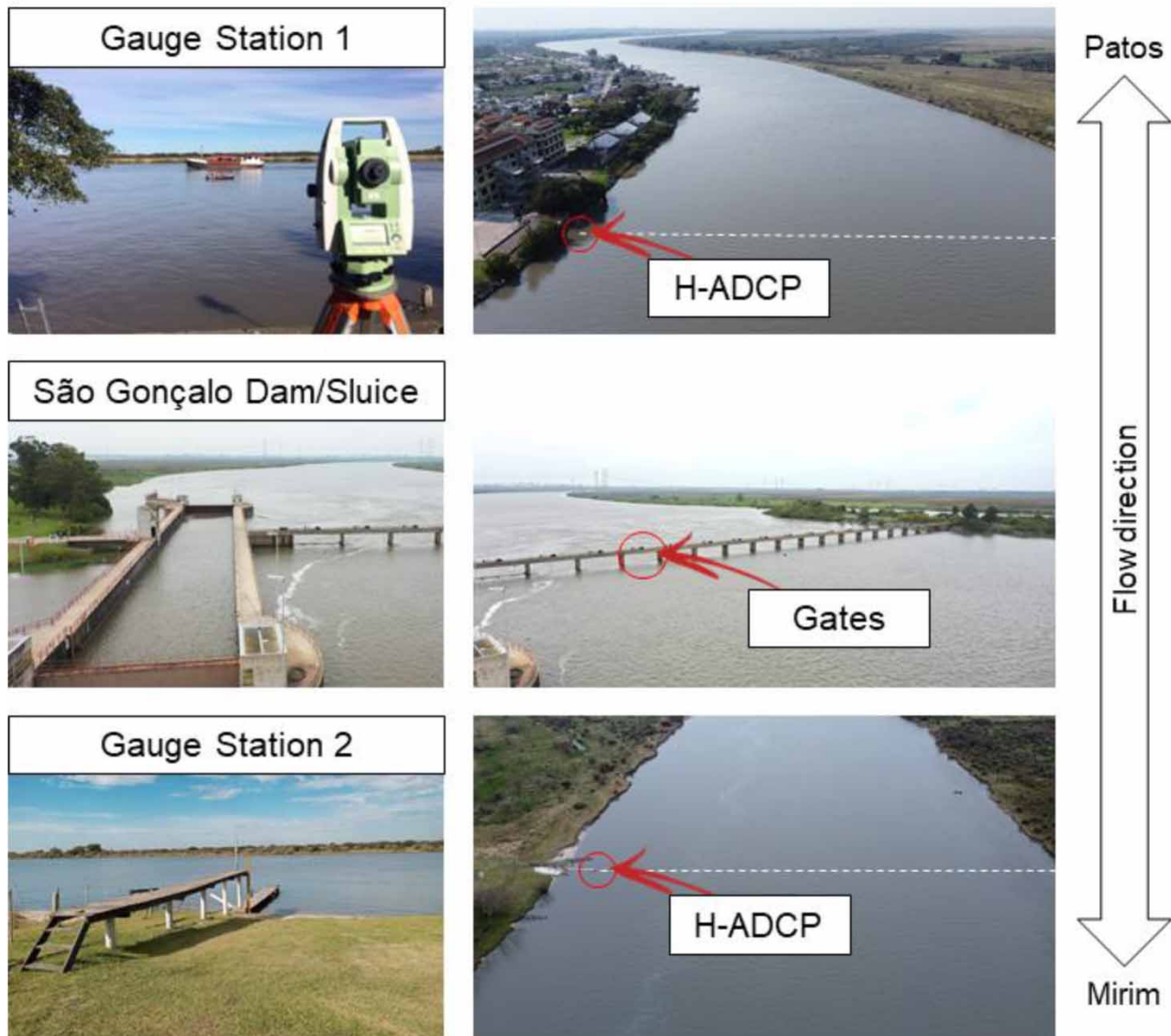


**Figure 3** | Overview of the GS1, São Gonçalo Dam/Sluice, and GS2. Highlighted are the H-ADCP locations, the 18 gates of the Dam/Sluice, and the predominant flow direction at the three sites.

instrument and energy system at GS1 and ~70 m at GS2), connected to a voltage controller to avoid voltage fluctuations. The H-ADCP is attached on a mobile iron structure, which allows the H-ADCP to be moved vertically, and this mobile structure moves over an iron support fixed at the left riverbank side wall and at the channel bed. The instrument operates recording in both IVC (~100 m) and multi-cell profile (10 m each) modes, at the same time (Figure 4). The data were recorded at 900-s intervals from averaging during 300 s. All the recorded data are processed and downloaded by the user using the software ViewArgonaut™. The setup configuration applied during GS1 and GS2 H-ADCPs installation is shown in Table 1.

It is worth noting that the blanking distance refers to the use of the multi-cell velocity (MCV) approach; cell begin refers to the use of the integrated velocity cell (IVC) (SonTek 2009), these being two completely different approaches, which consider different horizontal profile measured portions (Figure 4). The cross-sections' topobathymetry are presented in Figures 5(a) and 5(b), respectively, with the min/max stage observed during the studied period.

The MCV itself can look at each of the 10 cells along the cross-section from the two H-ADCP horizontal beams, allowing a more precise and discretized assessment of the  $x$ -axis velocity distribution over the horizontal profile. Considering the MCV,

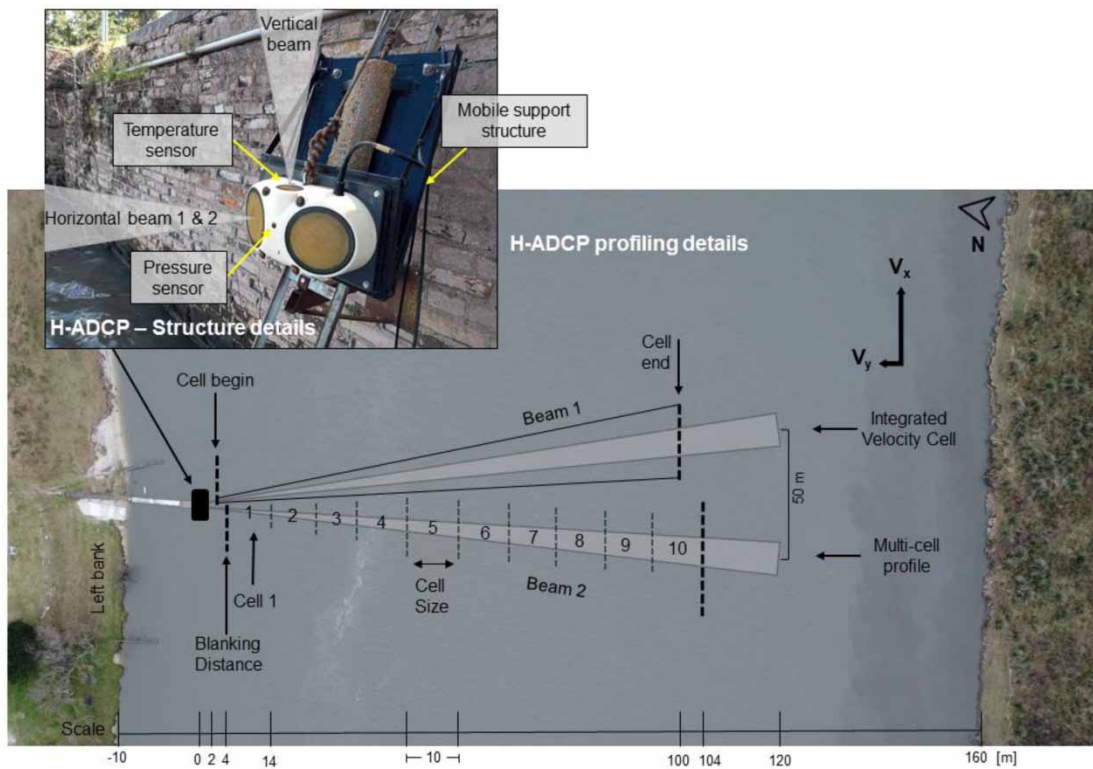


**Figure 4** | H-ADCP profiling details (distances refers to GS2) showing the IVC and MCV profile methods. In detail, H-ADCP structure and support installation.

**Table 1** | Aspects set up on GS1 and GS2 H-ADCPs

	GS1	GS2
Pitch [°]	-1.5	-0.8
Level [m]	-0.37	-0.34
Cell begin [m]	2	2
Cell end [m]	120	100
Cell size [m]	10	10
Blanking distance [m]	10	4

each cell from 1 to 10 is a mean value from beams 1 and 2, for example,  $x$ -axis velocity into Cell 4 is going to be the mean  $x$ -axis velocity from Cell 4 beam 1 and Cell 4 beam 2. The  $x$ -axis velocity of Cell 4 on GS2 (see Figure 4) is a 10-m long portion starting 34 m from the H-ADCP (considering blanking distance equals to 4 m + 10 m for each of the Cells 1–3), instead of the IVC which considers a 98 m portion along the cross-section (considering cell start and cell end as 2 m and 100 m, respectively).

The cross-sectional discharge at the gauge stations was also measured by a Dynamic Acoustic Doppler Current Profiler (D-ADCP). At GS1, there were 27 surveys between October 2015 and June 2019, and at GS2 there were 22 surveys between March 2019 and November 2019 (Table 2; Supplementary information, Tables S1 and S2). These D-ADCP data are only used on the IVRC development step which needs cross-section mean velocity ( $V_{D-ADCP}$ ) punctual data. The discharge measurements were carried out with a D-ADCP designed using a Sontek™/YSI RiverSurveyor™ M9 model, built-in with nine transducers,  $4 \times 3$  MHz and  $4 \times 1$  MHz both responsible for measuring the velocity and flow direction with  $0.002 \text{ m s}^{-1}$  accuracy, and  $1 \times 0.5$  MHz transducer for bathymetry purposes. In addition, the D-ADCP has a temperature sensor applied for

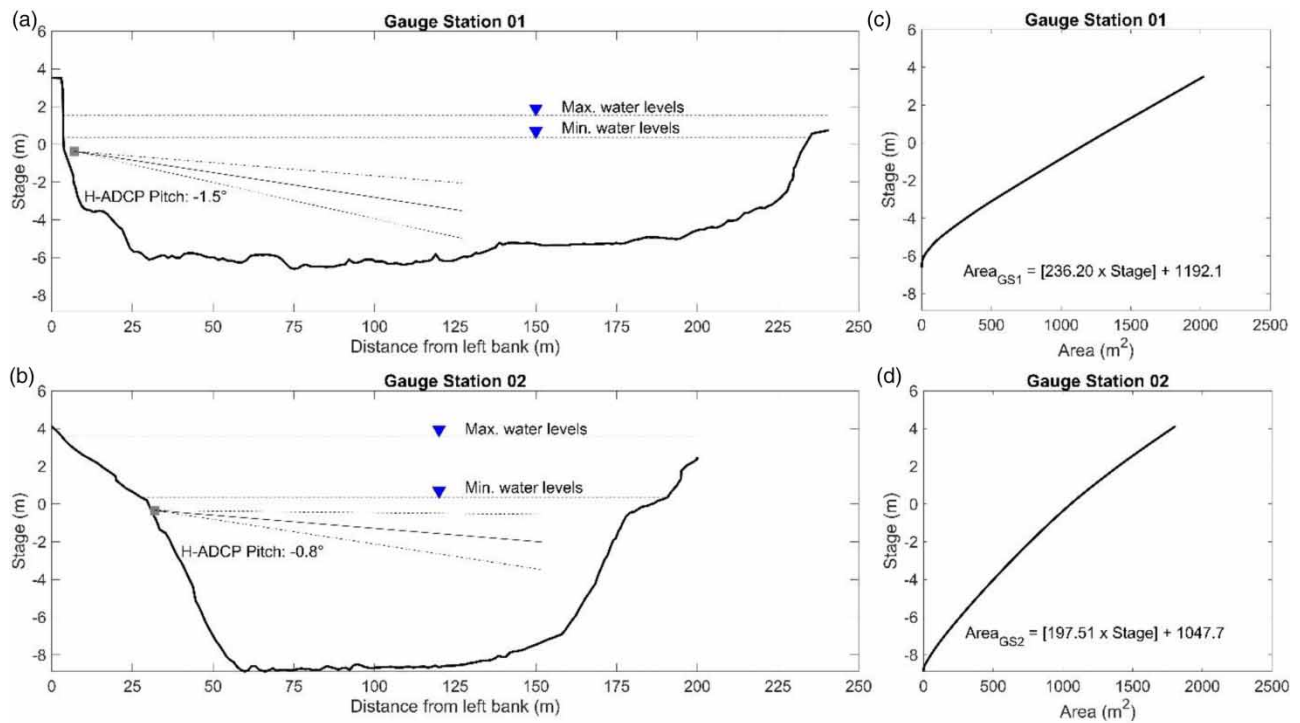


**Figure 5** | The cross-sections of the topobathymetric survey from (a) GS1, (b) GS2, with the H-ADCPs horizontal angles (pitch) of installation, and the stage–area rating curves for GS1, and GS2.

**Table 2** | Min/max discharges [ $\text{m}^3 \text{s}^{-1}$ ] and VD-ADCP [ $\text{m}\cdot\text{s}^{-1}$ ] observed for GS1 and GS2

	GS1		GS2	
	Discharge	$V_{D-ADCP}$	Discharge	$V_{D-ADCP}$
Minimum	157.21	0.12	-269.83	-0.25
Maximum	1,861.79	1.26	1,384.43	0.85

acoustic pulse velocity instantaneous correction, as well as an internal compass. To ensure data consistency, the measurements were post-processed by QRev™ software (Mueller 2016), which allows us to analyze deeply the collected velocity profiles. The D-ADCP collected data used bottom tracking as the reference for position. Following the recommendation by Mueller *et al.* (2013), each measurement was made by at least two pairs of reciprocal transects. Moreover, stationary moving-bed tests were performed on GS1 and GS2, under different flow conditions. On both sites no moving-bed characteristics were detected considering the discharge measurements performed, following criteria pointed out by Mueller *et al.* (2013).

### IVRC method

According to Rantz (1982b), the IVRC approach separates the cross-section area and the mean velocity; the cross-section area is obtained from observing the stage through a linear regression between these two; the flow velocity ( $V_{\text{mean}}$ ) is obtained from the relationship between the cross-section mean velocity ( $V_{D-ADCP}$ ) and the indexed velocity (it can be a random point at the cross-section, usually the  $x$ -axis velocity, perpendicular to the flow). While considering H-ADCPs, the indexed velocity ( $V_{\text{INDEX}}$ ) applied to the IVRC development may be the beam integrated velocity from cell begin to cell end (IVC), and it

may also be the discretized average velocity registered by a single cell or multiple cells (MCV), as illustrated in Figure 4. In turn, the  $V_{D-ADCP}$  and  $V_{INDEX}$  relationship is inherent for each studied cross-section, and it can consider the use of the IVC, the MCV, or  $MCV + IVC$  on the development of the IVRC.

The IVRC quality is dependent on the number of  $V_{D-ADCP}$  measurements performed and the variability of the hydraulic conditions observed, that is, the greater the number of measurements and the greater the variability observed (measurements in dry and flood season period, high stage, low flow velocity, high flow velocity, inverse flows, backwater, and bi-directional flows occurrence, etc.), the greater the capacity of the IVRC models to represent real flow conditions on the channel.

The assessment of the IVRC models was based on the mean absolute error (MAE) and the coefficient of determination ( $r^2$ ). Also, MAE and  $r^2$  were considered for the MCV cell selection at each gauge station. Further statistical performances from the best IVRC models developed are detailed in Supplementary Information, Table S3.

### Hydraulic variables

From the use of H-ADCP and D-ADCP, the necessary hydraulic variables for IVRC modeling, on both GS1 and GS2, were obtained. The  $V_{D-ADCP}$  from the D-ADCP measurements are only used for IVRC models development. The  $V_{INDEX}$  from the H-ADCP, even the MCV and IVC on the  $x$ -axis, is used for IVRC model developments and then for further  $V_{mean}$  estimations. The topobathymetric survey is only used for the stage  $\times$  area relationship and it was developed using the software AreaComp 1 – Version 1.13 (Lant & Mueller 2012) widely used from the United States Geological Survey (USGS) at their monitored stations, following good practices mentioned on Levesque & Oberg (2012). The stage is monitored by the H-ADCP (obtained from the pressure sensor/vertical beam) and further applied to estimate the cross-section wetted area (Figure 5).

To sum up the study collected data are as follows: (i) discharge measurements from the D-ADCP and (ii) post-process on QRev<sup>®</sup> to obtain the  $V_{D-ADCP}$ , then applied on IVRC-developing models; as well from the H-ADCP (iii) continuous  $V_{INDEX}$  was collected and (iv) post-processed on ViewArgonaut<sup>®</sup> to obtain IVC and MCV data, then applied on IVRC-developing models; while (v) the H-ADCP monitors the stage, and (vi) a topobathymetric survey was conducted, both (vii) applied to stage  $\times$  area rating curve developed using AreaComp software; the results are (viii) continuous  $V_{mean}$  estimated data and (ix) continuous area estimated data, then (x) multiplying these two results in an estimated discharge time-series for GS1 and GS2. The steps followed herein are presented in Figure 6 as a flowchart.

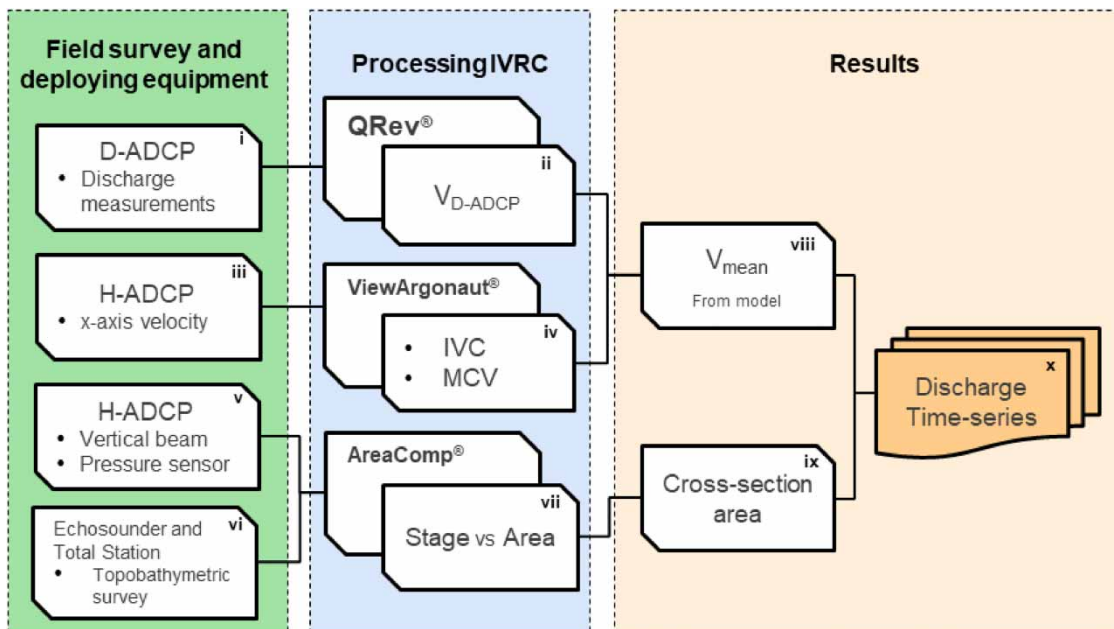


**Figure 6** | Main steps followed for data acquisition, data processing, and results generation.

## RESULTS

From the 27 D-ADCP surveys performed at GS1 and 22 performed at GS2, the maximum/minimum observed for discharge and  $V_{D-ADCP}$  are shown in Table 2.

These results show the D-ADCP discharge measurements were capable of covering a decent amplitude of data over the year. At GS2 some moments with negative flow and/or with stationary flow (4 and  $0.0042 \text{ m s}^{-1}$ ) were identified. Over the year, for both gauge stations, the flood period was identified between September and January, and the drought period between March and June.

The detailed information from each discharge measurement is in the Supplementary Information.

### SGC IVRC assessment

The relationship between  $V_{D-ADCP}$  and  $V_{INDEX}$  in both gauge stations was evaluated from three different IVRC approaches: (i) linear regression models considering the IVC method; (ii) linear regression models considering the MCV method; (iii) multiple linear regression models considering both IVC and MCV. As mentioned before, considering the MCV approach, the chosen cells were taken based on the smallest MAE and the  $r^2$  closest to 1 (see all the tested models and cell combinations/performances in Supplementary Information, Table S3). For GS1 and GS2, the best fit for each of the three applied approaches is shown in Figures 7 and 8. To identify and demonstrate the complex flow conditions occurring in the SGC, we also developed a linear regression between stage and  $V_{D-ADCP}$  (similar to a SQRC).

From the GS1 models (Figure 7), it seems the linear regression using stage (Figure 7(a)) as a predictor variable has shown the worst performance when compared to the others, resulting in an MAE of  $0.194 \text{ m s}^{-1}$  and  $r^2$  of 0.534. However, the IVC and MCV models (Figures 7(b) and 7(c)) both presented similar results with small error (MAE of 0.032 and  $0.017 \text{ m s}^{-1}$ , respectively) and  $r^2$  of 0.986 and 0.996, respectively. However, the best fit model was obtained when considering MVC + IVC (Cell 2 and Cell 6, Figure 7(d)) in a multiple linear regression model, with  $r^2$  of 0.998 and an MAE of  $0.012 \text{ m s}^{-1}$ . Comparing the MCV + IVC model, it represents an MAE of 90% less than the SQRC approach, MAE 60% less than the IVC model, and MAE 30% less than the MCV model itself.

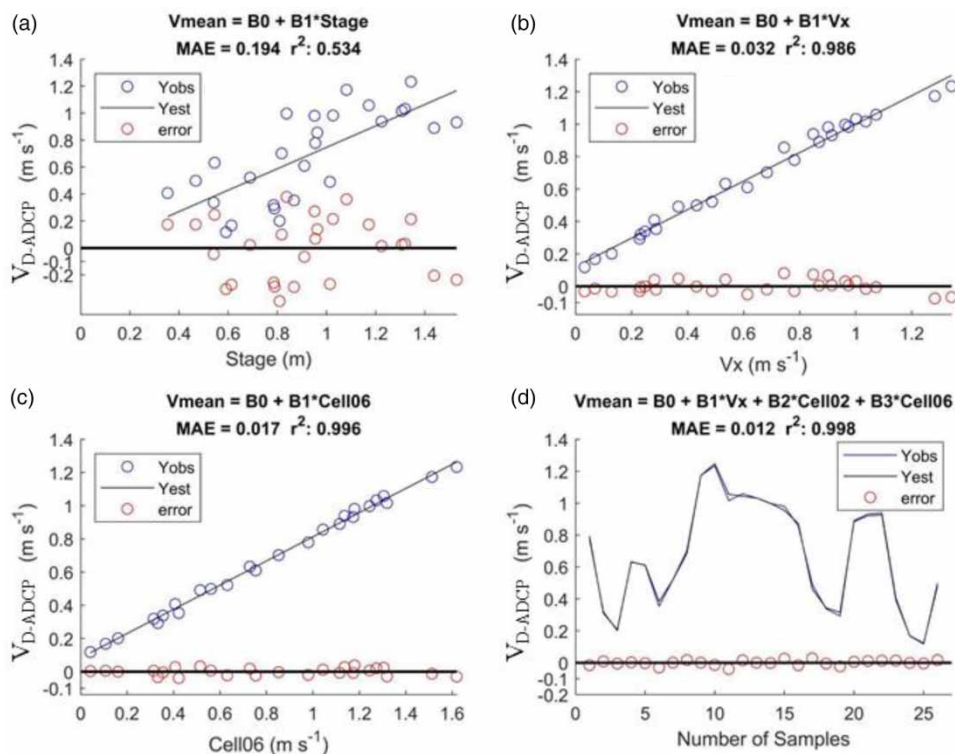


**Figure 7** | Regression models to estimate the mean velocity for GS1 using (a) stage (similar to a SQRC), (b)  $V_{INDEX}$  (considering IVC), (c)  $V_{INDEX}$  in Cell 6 (considering MCV), and (d)  $V_{INDEX}$  on IVC and also the Cells 2 and 6.

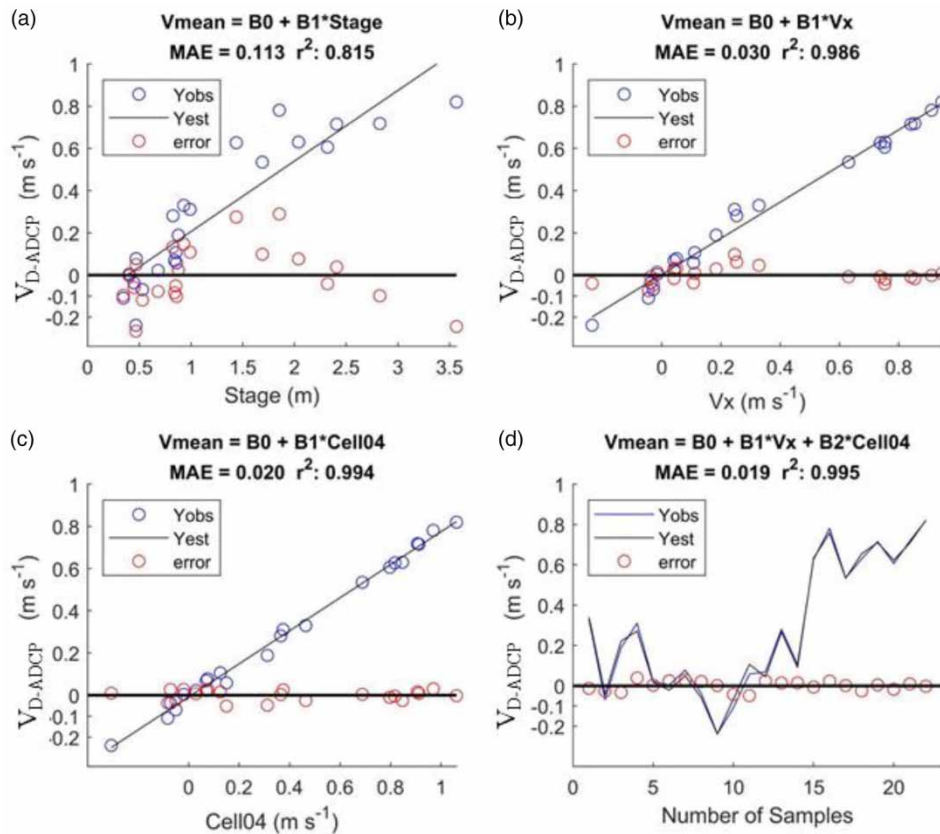


**Figure 8** | Regression models to estimate the mean velocity for GS2 using (a) stage (similar to a SQRC), (b)  $V_{INDEX}$  (considering IVC), (c)  $V_{INDEX}$  in Cell 4 (considering MCV), and (d)  $V_{INDEX}$  on IVC and also the Cell 4.

At the GS2, the IVRC model considering stage (Figure 8(a)) as a predictor variable performed worst, showing asymmetric error distribution and hysteresis effects, as well as an MAE of  $0.113 \text{ m s}^{-1}$  and  $r^2$  of 0.815. However, the GS2 IVRC models result considering the IVC (Figure 8(b)), MCV (Figure 8(c)), and MCV + IVC (Cell 4 - Figure 8(d)) presented better results compared to the stage approach (Figure 8(a)). For GS2, the best fit was the IVRC model performed from multiple linear regression with two predictor variables (MCV + IVC considering the Cell 4), which presented an MAE 80% less than the SQRC approach, MAE 37% less than the IVC model, and MAE 5% less than the MCV model itself.

More details from each of the developed models for GS1 and GS2 are presented in the Supplementary Information.

### Discharge time-series

The stage,  $V_{INDEX}$  considering IVC,  $V_{INDEX}$  considering MCV, and discharge time-series for GS1 and GS2 are shown in Figures 9 and 10, respectively. The lack of information on both gauges is due to the problems that both H-ADCPs presented during the monitored period, such as power cord and data loggers problems. Given the complex flow conditions at SGC, it is reasonable not to use any method for gap-filling the missing data.

The H-ADCP estimated discharge time-series for GS1 (Figure 9(d)) had fitted in the min/max D-ADCP discharge measurements for almost the entire period, suggesting the SGC variations were covered almost totally.

The results suggest that, for GS1, the IVRC model had performed significantly. The minimum and maximum discharge estimations from the MCV + IVC model (Figure 9(d) - red line) were  $43.211$  and  $1,980.017 \text{ m}^3 \text{ s}^{-1}$ , respectively, and the minimum and maximum discharge estimations from the IVC model (Figure 9(d) - black line) were  $78.881$  and  $1,967.831 \text{ m}^3 \text{ s}^{-1}$ , respectively. In both situations no periods of inversive flow were registered.

At GS2, the H-ADCP discharge estimations (Figure 10(d)) had fitted in the min/max D-ADCP discharge measurements for almost the entire period, even though the D-ADCP data are concentrated in the first half of the analyzed period. The results of the time-series suggest that the SGC variations were covered totally.

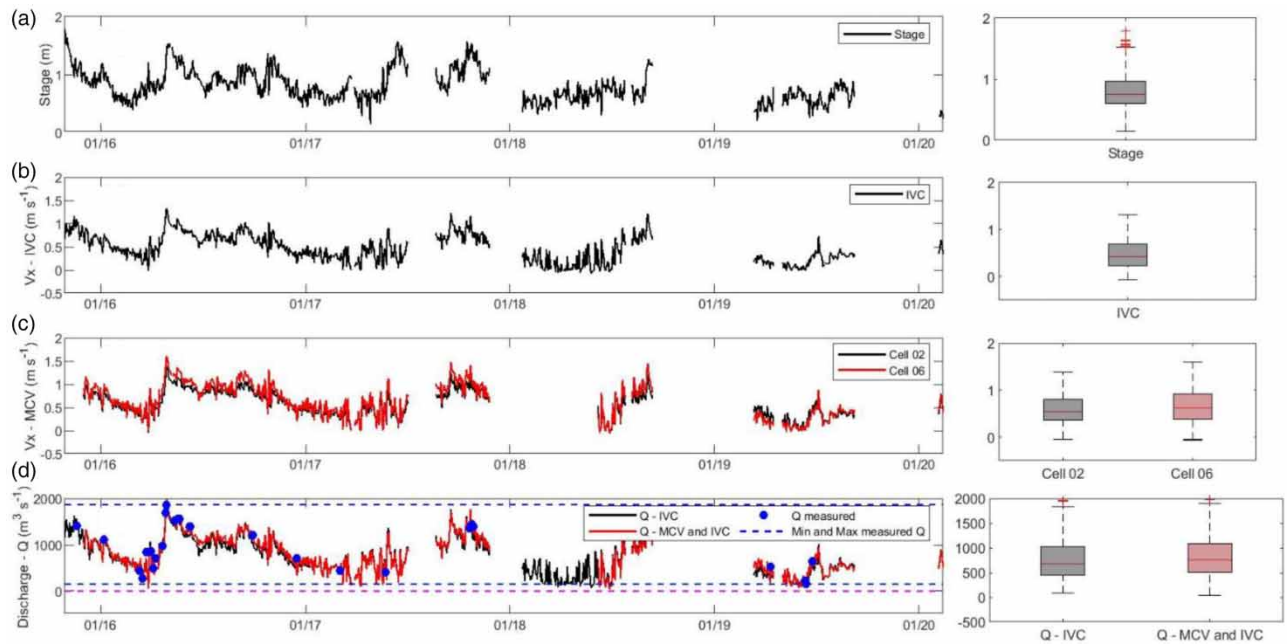


**Figure 9** | Time-series and box plots representing data variation developed for GS1 showing (a) stage, (b)  $V_{INDEX}$  (considering IVC), (c)  $V_{INDEX}$  in Cell 2 and Cell 6 (considering MCV), (d) discharges applying IVC and MCV + IVC. Please refer to the online version of this paper to see this figure in color: <http://dx.doi.org/10.2166/hydro.2023.045>.

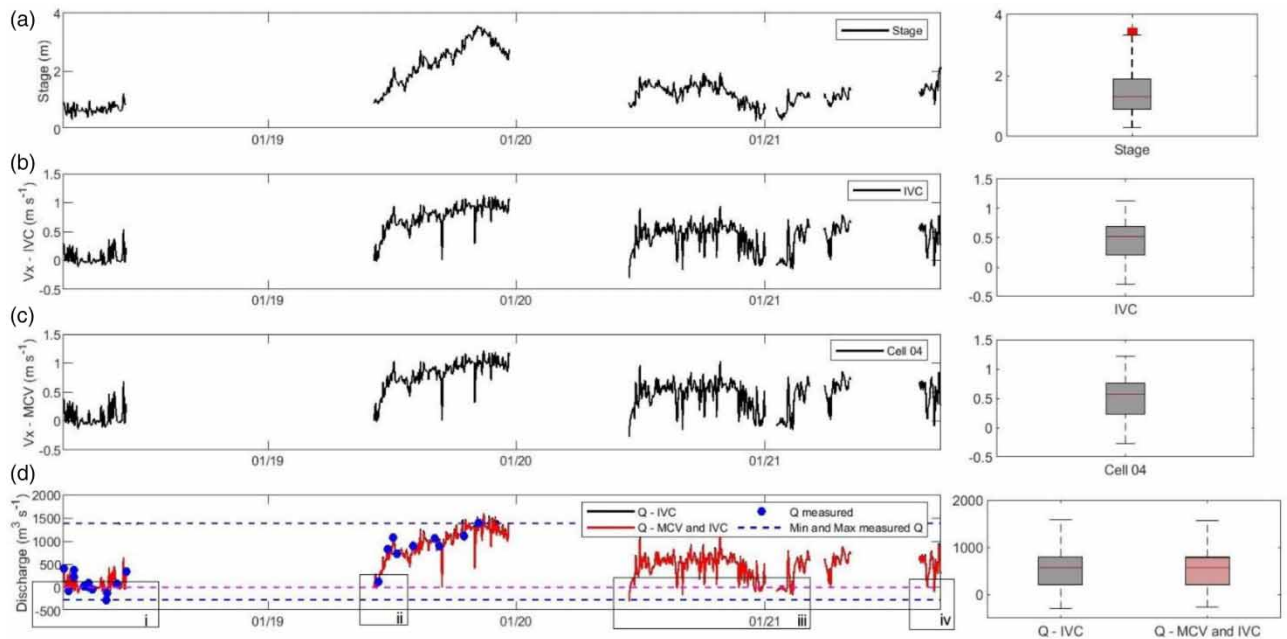


**Figure 10** | Time-series and box plots representing data variation developed for GS2 showing (a) stage, (b)  $V_{INDEX}$  (considering IVC), (c)  $V_{INDEX}$  in Cell 4 (considering MCV), (d) discharges applying IVC and MCV + IVC. Highlighted four inverse flow moments captured.

The results herein found for GS2 clearly suggest that the IVRC model had performed significantly with minimum and maximum discharge estimations from the MCV + IVC model (Figure 10(d) – red line) as  $-270.675$  and  $1,570.650 \text{ m}^3 \text{ s}^{-1}$ , respectively, as well as the minimum and maximum discharge estimations from the IVC model (Figure 10(d) – black line) as  $-296.727$  and  $1,590.758 \text{ m}^3 \text{ s}^{-1}$ , respectively.

At GS2, the results pointed out four main moments with negative discharge estimation values, with the minimum framed as (i)  $-122.9 \text{ m}^3 \text{ s}^{-1}$ , (ii)  $-22 \text{ m}^3 \text{ s}^{-1}$ , (iii)  $-270.7 \text{ m}^3 \text{ s}^{-1}$  (the maximum inversive flux registered in this study), (iv)  $-147.2 \text{ m}^3 \text{ s}^{-1}$  (Figure 10(d)). At none of the four inversive flow moments did the stage variable register negative values.

### Observed $\times$ estimated regression for discharge values

The relationship between observed (D-ADCP discharge) and estimated (H-ADCP discharge from the best fit IVRC model) values and its residuals are next presented for GS1 and GS2 (Figure 11). For the GS1, the IVRC model applied is the one which considers the MCV + IVC (Cells 2 and 6) model, as presented in Figure 7(d). For the GS2, the IVRC model applied is the one which considers the MCV + IVC (Cell 4) model, as presented in Figure 8(d).

The results of residuals from the relationship between observed and estimated discharges at GS1 (Figure 11) had shown homogeneous residual distribution for low and high flow discharges, with an MAE of  $16.864 \text{ m}^3 \cdot \text{s}^{-1}$  (1.71% of the mean, 0.90% of the maximum, and 10.33% of the minimum estimated discharges for observed moments), with  $43.211 \text{ m}^3 \cdot \text{s}^{-1}$  as the minimum estimated in this study by the MCV + IVC model at GS1.

At GS2, the residual (Figure 11) from the relationship between observed and estimated discharges showed a homogeneous distribution with an MAE of  $23.414 \text{ m}^3 \cdot \text{s}^{-1}$  (5.60% of the mean, 1.69% of the maximum, and 8.64% of the minimum estimated discharges for observed moments), with  $-270.675 \text{ m}^3 \cdot \text{s}^{-1}$  as the minimum estimated in this study by the MCV + IVC model at GS2.

## DISCUSSION

The D-ADCP surveys performed to obtain *in situ* discharge measurements were conducted in both monitored gauge stations during the period of November 2015–2019, comprising a total of 49 campaigns (Table 1, SP1 and SP2) and covering most of the hydraulic situations that occur at the SGC, as flood/drought moments and bi-directional/stationary flows. The amplitude of discharge measurements helps improve the performance of the IVRC models, for example, on the development of the GS2 IVRC models which considered negative D-ADCP discharge measurements ( $-41.761$ ,  $-269.83$ , and  $-120.938 \text{ m}^3 \text{ s}^{-1}$ ), registering the occurrence of inversive flows, typical from complex flow channels.

From the IVRC-developed models (shown in Figures 7 and 8), the MCV + IVC approach showed better performance compared to the IVC approach, noticed in GS1 and GS2. The SQRC showed the worst performance compared to MCV + IVC and IVC models at GS1 and GS2. Thus, the results clearly suggest that the use of SQRC models is not ideal for the SGC

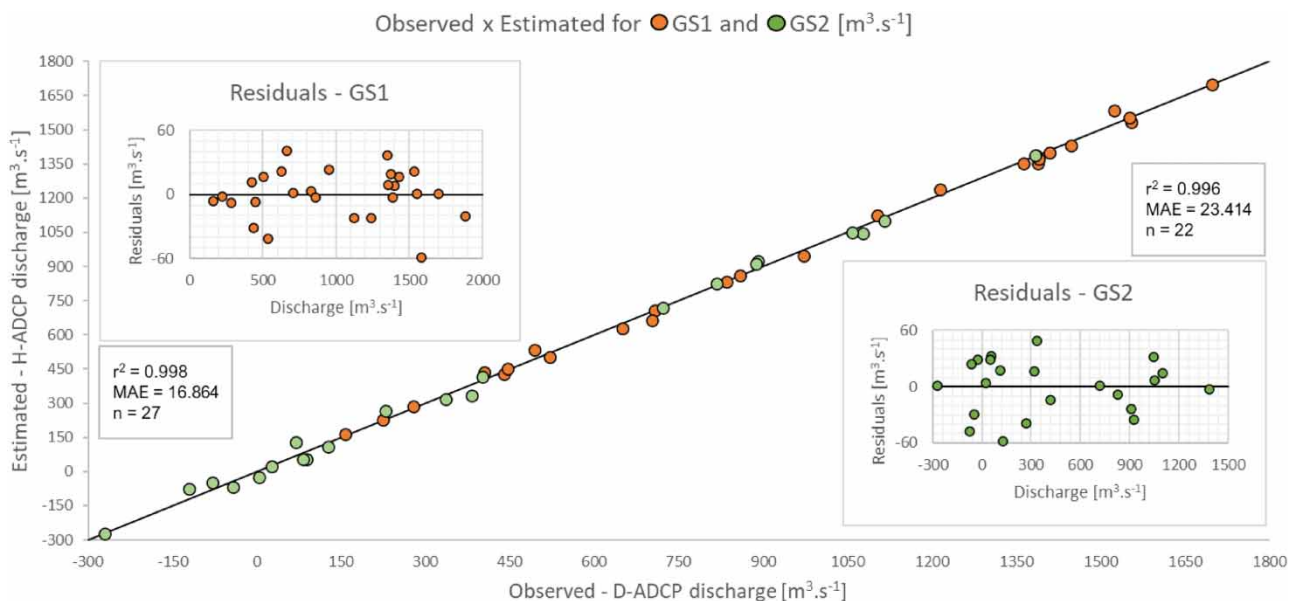


**Figure 11** | Regression between observed (D-ADCP surveys) and estimated (for H-ADCP from the best fit model) discharge values and their residuals for GS1 and GS2.

characteristics and its complex flow conditions, despite prior studies (Oliveira *et al.* 2015; Jung *et al.* 2020), due to the inability of the SQRC approach in estimating good discharges in moments with bi-directional/inversive flow, which occurs in SGC.

Still from the IVRC models, in addition to the small error presented from the IVC and/or MCV + IVC approaches (Figures 7 and 8), its distribution is quite symmetrical for low and high flow velocities, and it is corroborated by the relationship between observed and estimated discharge values and its residues (Figure 11), which has shown a homogeneous residual distribution with an MAE of  $16.864 \text{ m}^3 \text{ s}^{-1}$  for GS1 and  $23.414 \text{ m}^3 \text{ s}^{-1}$  for GS2. This fact demonstrates the efficiency of applying the three approaches for the IVRC model development to estimate the  $V_{\text{mean}}$  and then estimate discharges in both gauge stations.

From the time-series results, the discharge estimations applying IVRC models on both gauge stations presented reasonable performance. The time-series was capable of estimating discharges under the whole amplitude of SGC hydraulic conditions and *in situ* observed discharge data. The similarity of model performances when considering the IVC and MCV + IVC approaches allows the user to choose between these while guaranteeing a high degree of certainty (Figures 9(d) and 10(d)), even when out of observed data moments.

What was found here makes it clear that the GS2 discharge estimation time-series from the analyzed period can represent more comprehensive flow conditions compared to the other studies carried out in the SGC, with registered negative flows at GS2, that is, flow direction from Patos toward Mirim, as highlighted in Figure 10(d). According to a study done by Oliveira *et al.* (2015), these authors performed discharge measurements at GS2 and found positive discharges from 98.54 up to  $1,503 \text{ m}^3 \text{ s}^{-1}$  during the period between January 2009 and December 2011. In another study, Oliveira *et al.* (2019) had found a flow discharge range from 300 up to  $2,250 \text{ m}^3 \text{ s}^{-1}$  analyzing in the year 2002, but nonetheless its results are obtained from modeling in the SGC. Despite the maximum values described in prior studies, we have found no conclusive evidence that these discharge magnitudes really occur at SGC, either from the D-ADCP measurements or the H-ADCP registered data.

## CONCLUSIONS

From the developed models, a time-series for predicted discharges for the two gauge stations in SGC was generated with a high degree of certainty. They are based on the IVRC principles and applied to estimate mean flow velocity, using the hydraulic variables monitored from an H-ADCP. The IVRC models considered the  $V_{\text{INDEX}}$  as IVC in the horizontal beam (IVC approach), and the  $V_{\text{INDEX}}$  as discretized MCV (MCV approach), both on  $x$ -axis direction, through linear and multiple linear regression models. The rating curve traditional approach, which is based only on stage to predict the discharge, is not representative for the SGC, and is therefore not applicable under these conditions.

All three IVRC development methods presented good performances in estimating mean flow velocity at both gauge stations. We highlight the better performance from the combined use of IVC and MCV for developing IVRC multiple linear regression models. In these IVRC models, we have found smaller errors, in addition to a symmetrical distribution of errors, both for low and high flow velocities. Based on these assumptions, for the reproducibility of this work, we suggest that other authors take note if there is no interference at any point of the beams such as contact with the river/channel bed and/or water surface, which may invalidate the use of some cells; as well as trying all the valid cells combinations to find a better IVRC performance.

For the analyzed period, it was possible to register moments with inversive flows, even during D-ADCP discharge measurements and during H-ADCP discharge monitoring (after applying the best fit IVRC model for discharge estimations), evidencing the better performance of the IVRC approach over the SQRC approach and the SGC complex characteristics.

Due to the results, we strongly suggest keeping the hydraulic variables monitored at the SGC. Primarily, to better understand its complex water behavior, and better develop IVRC understanding from natural and complex channels, which is only possible with long-term monitoring of flow characteristics.

## ACKNOWLEDGEMENTS

We thank NEPE-HidroSedi at the Federal University of Pelotas (UFPel) for field surveys using the D-ADCP and providing the time-series obtained with the H-ADCP. We thank the Mirim-São Gonçalo Basin Development Agency for proposing the study theme that is so important for better understanding the complex hydrodynamics of the SGC. L.S.L. received support from the Coordenação de Aperfeiçoamento de Pessoal de Nível Superior – Brasil (CAPES) – Finance Code 001.

## DATA AVAILABILITY STATEMENT

All relevant data are included in the paper or its Supplementary Information.

## CONFLICT OF INTEREST

The authors declare there is no conflict.

## REFERENCES

- Benson, M. A. & Dalrymple, T. 1967 *General Field and Office Procedures for Indirect Discharge Measurements*. U.S. G.P.O., Washington, DC. [https://pubs.usgs.gov/twri/twri3-a1/twri\\_3-A1\\_a.pdf](https://pubs.usgs.gov/twri/twri3-a1/twri_3-A1_a.pdf)
- Chen, Y. C., Yang, T. M., Hsu, N. S. & Kuo, T. M. 2012 Real-time discharge measurement in tidal streams by an index velocity. *Environmental Monitoring and Assessment* **184**, 6423–6436. <https://doi.org/10.1007/s10661-011-2430-y>.
- Cheng, Z., Lee, K., Kim, D., Muste, M., Vidmar, P. & Hulme, J. 2019 Experimental evidence on the performance of rating curves for continuous discharge estimation in complex flow situations. *Journal of Hydrology* **568**, 959–971. <https://doi.org/10.1016/j.jhydrol.2018.11.021>.
- Costi, J., Marques, W. C., Kirinus, E. d. P., Duarte, R. d. F. & Arigony-Neto, J. 2018 Water level variability of the Mirim – São Gonçalo system, a large, subtropical, semi-enclosed coastal complex. *Advances in Water Resources* **117**, 75–86. <https://doi.org/10.1016/j.advwatres.2018.05.008>.
- Dias, L. C., Fernandes, L. L. & Lopes, D. F. 2019 Development and extrapolation of rating curves in Amazon. *Revista Brasileira de Geografia Física* **12**, 2285–2301.
- Farahmand, T. & Hamilton, S. 2016 *Computing Continuous Record of Discharge with Quantified Uncertainty Using Index Velocity Observations: A Probabilistic Machine Learning Approach*. Geophysical Research Abstracts.
- Fiandrino, A., Ouisse, V., Dumas, F., Lagarde, F., Pete, R., Malet, N., le Noc, S. & de Wit, R. 2017 Spatial patterns in coastal lagoons related to the hydrodynamics of seawater intrusion. *Marine Pollution Bulletin* **119**, 132–144. <https://doi.org/10.1016/j.marpolbul.2017.03.006>.
- Friedrich, A. C., Niencheski, L. F. & Santos, I. R. 2006 Dissolved and particulate metals in Mirim Lagoon. *Brasil-Uruguayan Border. Journal of Coastal Research SI* **39**, 1036–1039.
- Jung, B. M., Fernandes, E. H., Möller, O. O., Jr. & García-Rodríguez, F. 2020 Estimating suspended sediment concentrations from river discharge data for reconstructing gaps of information of long-term variability studies. *Water* **12**, 2382. <https://doi.org/10.3390/w12092382>
- Kästner, K., Hoitink, A. J. F., Torfs, P. J. J. F., Vermeulen, B., Ningsih, N. S. & Pramulya, M. 2018 Prerequisites for accurate monitoring of river discharge based on fixed-location velocity measurements. *Water Resources Research* **54**, 1058–1076. <https://doi.org/10.1002/2017WR020990>.
- Kjerfve, B. 1994 Coastal Lagoons. In: *Elsevier Oceanography Series, Vol. 60* (B. Kjerfve, ed.). Elsevier, Amsterdam, pp. 1–8.
- Lant, J. & Mueller, D. S. 2012 *Stage Area Rating Application-AreaComp2*.
- Le Coz, J., Pierrefeu, G. & Paquier, A. 2008 Evaluation of river discharges monitored by a fixed side-looking Doppler profiler. *Water Resources Research* **46**. <https://doi.org/10.1029/2008WR006967>.
- Levesque, V. A. & Oberg, K. A. 2012 *Computing Discharge Using the Index Velocity Method*. U.S. Dept. of the Interior, U.S. Geological Survey, Reston, Virginia.
- Mueller, D. S. 2016 *QRev-Software for Computation and Quality Assurance of Acoustic Doppler Current Profiler Moving-Boat Streamflow Measurements-User's Manual for Version 2.8*. Reston, Virginia. <https://doi.org/10.3133/ofr20161052>.
- Mueller, D. S., Wagner, C. R., Rehmel, M. S., Oberg, K. A. & Rainville, F. 2013 *Measuring Discharge with Acoustic Doppler Current Profilers from a Moving Boat*. Reston, Virginia. <https://doi.org/10.3133/tm3A22>.
- Munar, A. M., Cavalcanti, J. R., Bravo, J. M., Fan, F. M., Motta-Marques, D. d. & Fragoso, C. R. 2018 Coupling large-scale hydrological and hydrodynamic modeling: toward a better comprehension of watershed-shallow lake processes. *Journal of Hydrology* **564**, 424–441. <https://doi.org/10.1016/j.jhydrol.2018.07.045>.
- Munar, A. M., Cavalcanti, J. R., Bravo, J. M., da Motta-Marques, D. & Fragoso, C. R. 2019 Assessing the large-scale variation of heat budget in poorly gauged watershed-shallow lake system using a novel integrated modeling approach. *Journal of Hydrology* **575**, 244–256. <https://doi.org/10.1016/j.jhydrol.2019.05.025>.
- Muste, M. & Hoitink, T. 2017 Measuring Flood Discharge. In: *Oxford Research Encyclopedia of Natural Hazard Science*. Oxford University Press. <https://doi.org/10.1093/acrefore/9780199389407.013.121>.
- Muste, M., Lee, K., Kim, D., Bacotiu, C., Oliveros, M. R., Cheng, Z. & Quintero, F. 2020 Revisiting hysteresis of flow variables in monitoring unsteady streamflows. *Journal of Hydraulic Research* **58**, 867–887. <https://doi.org/10.1080/00221686.2020.1786742>.
- MVOTMA 2017 *Plan Nacional de Aguas*.
- Oliveira, H. A. d., Fernandes, E. H. L., Möller, O. O. J. & Collares, G. L. 2015 Hidrology and hydrodynamics of Mirim Lagoon. *Revista Brasileira de Recursos Hídricos* **20**, 34–45.
- Oliveira, H., Fernandes, E., Möller, O. & García-Rodríguez, F. 2019 Relationships between wind effect, hydrodynamics and water level in the world's largest coastal lagoonal system. *Water (Switzerland)* **11**. <https://doi.org/10.3390/w11112209>.

- Peel, M. C., Finlayson, B. L. & McMahon, T. A. 2007 Updated world map of the Köppen-Geiger climate classification. *Hydrology and Earth System Sciences* **11**, 1633–1644.
- Possa, T. M., Collares, G. L., Boeira, L. d. S., Jardim, P. F., Fan, F. M. & Terra, V. S. S. 2022 Fully coupled hydrological–hydrodynamic modeling of a basin–river–lake transboundary system in Southern South America. *Journal of Hydroinformatics*. <https://doi.org/10.2166/hydro.2021.096>.
- Rantz, S. E. 1982a *Measurement and Computation of Streamflow: Volume 1. Measurement of Stage and Discharge*. U.S. G.P.O., Washington, DC. <https://pubs.er.usgs.gov/publication/wsp2175>.
- Rantz, S. E. 1982b *Measurement and Computation of Streamflow: Volume 2. Computation of Discharge*. U.S. G.P.O., Washington, DC.
- SEMA 2021 *Secretaria do Meio Ambiente e Infraestrutura [Infrastructure and Environment Bureau] [WWW Document]*. Available from: <https://www.sema.rs.gov.br/1040-bh-mirim> (accessed 17 January 2022).
- Silva, D. V. d., Oleinik, P. H., Costi, J., Kirinus, E. d. P. & Marques, W. C. 2019 Residence time patterns of Mirim Lagoon (Brazil) derived from two-dimensional hydrodynamic simulations. *Environmental Earth Sciences* **78**. <https://doi.org/10.1007/s12665-019-8162-y>.
- SonTek 2009 *Argonaut-SL System Manual Firmware Version 12.0*. San Diego, California.
- Toldo Jr., E. 1994 *Sedimentação, Predição do Padrão de Ondas, e Dinâmica Sedimentar da Antepraia e Zona de Surfe do Sistema Lagunar*. Instituto de Geociências, Universidade Federal do Rio Grande do Sul, Porto Alegre.
- Vieira, H. M., Weschenfelder, J., Fernandes, E. H., Oliveira, H. A., Möller, O. O. & García-Rodríguez, F. 2020 Links between surface sediment composition, morphometry and hydrodynamics in a large shallow coastal lagoon. *Sedimentary Geology* **398**. <https://doi.org/10.1016/j.sedgeo.2020.105591>.
- Vougioukas, S., Papamichail, D., Georgiou, P. & Papadimos, D. 2011 River discharge monitoring using a vertically moving side-looking acoustic Doppler profiler. *Computers and Electronics in Agriculture* **79**, 137–141. <https://doi.org/10.1016/j.compag.2011.09.004>.
- WMO 1980 *Manual on Stream Gauging*. Geneva.

First received 28 March 2022; accepted in revised form 21 December 2022. Available online 10 January 2023